Research Square

Preprints are preliminary reports that have not undergone peer review.
They should not be considered conclusive, used to inform clinical practice,
or referenced by the media as validated information.

Research on grinding force modeling and surface morphology characteristics evaluation in dry grinding of Ti-6Al-4V machined by structured grinding wheel

Yao Sun
Tianwei He
Northeastern University
Zhen Hui
138490049810163.com

State Key Laboratory for High Performance Tools
Benjia Tang
Northeastern University
BinTong Zhao
Jiahao Gao
Yidi Wang
Qigen Peng
Northeastern University
Changyi Dong

Research Article

Keywords: Dry grinding, Grinding force, Surface topography, Ti-6Al-4V

Posted Date: November 13th, 2026

DOI: https://doi.org/10.21203/rs.3.rs-11062152/v1

License: This work is licensed under a Creative Commons Attribution 4.0 International License.
Read Full License

[Title Page]

Article Title

Research on grinding force modeling and surface morphology characteristics evaluation in dry grinding of Ti-6Al-4V machined by structured grinding wheel

Authors

Yao Sun[1,2], Tianwei He[2], Benjia Tang[2], Zhen Hui*[1],Bintong Zhao[2],Jiahao Gao[2],

Yidi Wang[3] , Qigen Peng[2], Changyi Dong[2]

Author affiliations:

[1] State Key Laboratory for High Performance Tools, Zhengzhou Research Institute for Abrasives & Grinding Co. LTD, 450000, P.R. China

[2] School of Mechanical Engineering and Automation, Northeastern University, Shenyang, 110819, China;

[3] General Technology Group machine tool Engineering Research Institute Co., LTD Shenyang branch, Shenyang, 110819, China.

*** Corresponding author name and information:**

Zhen Hui, Email address:13849004981@163.com

Yao Sun, Email address:sy547515291@163.com

(Check the Guide for authors to see the required information on the title page)

Research on grinding force modeling and surface morphology characteristics evaluation in dry grinding of Ti-6Al-4V machined by structured grinding wheel

Abstract

Dry grinding eliminates the use of coolant, reducing environmental pollution and energy consumption, which aligns with the green manufacturing principles of modern industry. However, dry grinding of titanium alloys presents issues such as high grinding forces, surface burning, and increased surface roughness. The design of structured grinding wheels can reduce friction and heat generation during the grinding process, thereby lowering grinding forces and temperatures, which helps to prevent surface burning and cracking resulting in better surface quality. By integrating the curved quadrilateral pyramid grit model, the material properties of titanium alloy TC4, and the surface structural parameters of a regular array structured grinding tool, a theoretical model for grinding force considering instantaneous contact state between the grit and the workpiece has been established. The mapping relationship between grinding forces, surface structural features of grinding tool, and processing parameters was explored. The research findings are of great significance in improving the surface quality of titanium alloy dry grinding with structured tools, enhancing processing efficiency, increasing process stability, promoting environmental protection, and expanding application fields.

Keywords: Dry grinding; Grinding force; Surface topography;Ti-6Al-4V;

1.Introduction

Titanium alloy is an alloy material made of titanium mixed with other metals, which has high strength, heat resistance and corrosion resistance, which makes titanium alloy have been widely used in the national economy, especially in the field of aerospace and biomedical fields [1-2].Besides, with advancements in science and technology and continuous improvement of product performance, and the higher requirements are put forward for the dimensional accuracy and surface quality of titanium alloy components[3-4]. However, the poor creep resistance, small elastic modulus and poor thermal conductivity of titanium alloy results in a lot of difficulties have been encountered in grinding titanium alloys, and the primary problems encountered in grinding titanium alloy can be summarized as large grinding force, high grinding temperature, serious tool wear and intensified hardening, etc [5-6].

The grinding force signal is a crucial parameter reflecting the state of the grinding process. By real-time monitoring and analysis of the grinding force signal, the stability and efficiency of the grinding process can be understood, and potential issues such as grinding wheel wear and workpiece deformation can be promptly identified and resolved. The study of grinding force signals holds significant importance for advancing the development of grinding technology. In-depth research into grinding force signals can reveal the physical and chemical mechanisms during the grinding process, providing theoretical support for the development of new grinding wheel materials, grinding techniques, and equipment[7-8]. By measuring and analyzing the force signals can understand changes in working conditions and optimize machining parameters accordingly. Thus, several scholars at home and abroad have conducted research on machining force signals. Niu et al.[9] found that cutting force signals are

more sensitive to tool wear than vibration and sound signals and experimentally proved that the classification accuracy of cutting force sensor-based wear monitoring model is 96.7%. Jemielniak et al. [10] studied that the cutting force sensing system was interfered by table resonance and proposed a multi-sensor fusion strategy to improve the system performance and avoid distorted single-feature information. Nogi et al.[11] proposed the new approach to combine high-frequency information with differential features, which is processed using a long and short-term memory model and significantly reduces the detection delay. Experiments demonstrated that this method outperforms feedforward neural and convolutional neural network. Sakaino et al. [12] proposed a force estimation method based on frequency analysis to deal with accurate force monitoring in noisy machining, which overcome the limitations of traditional force sensors and verify its effectiveness and robustness. Qin et al.[13] developed the titanium alloy helical milling force model based on parallel mechanism and can monitor the cutting force signals in real time, improve the machining stability by adjusting the parameters, and verify the model accuracy by time-frequency transformation. Xavier et al.[14]predicted the metal layer burr height in CFRP drilling by fractal analysis of cutting force signals and measured the burr height at the exit of the metal layer to verify that his monitoring method was effective and accurate. Kwak et al. [15] processed cutting force signals using discrete wavelet transform, extracted key features and detected the wheel re-dressing time and vibration onset of chattering for supporting the stable operation of automated manufacturing systems. Wang et al.[16] established the relationship model of grinding force with temperature and burns, monitoring the grinding force can predict the temperature change and prevent burns. Sutowski et al.[17]pointed out that grinding force amplitude changes can reflect cutting capacity and removal efficiency and the

monitoring force changes can be used to infer workpiece quality and grinding wheel life. Jamshidi et al.[18] monitored tool wear in drilling of CFRP and titanium stacked materials through fractal analysis of cutting force time series data to assess and prevent low quality machining in real time to ensure machining quality and efficiency.

Grinding force is caused by the elastic deformation, plastic deformation, chip formation, and friction between the grinding particle and workpiece after the contact of the grinding wheel with the workpiece, which is closely related to the integrity of the grinding surface. Grinding force has a significant relationship with the generation of grinding heat and vibration during the grinding process. At the same time, grinding force can cause plastic deformation of metal and produce residual stress, which in turn leads to damage to the grinding surface and subsurface. Tasi et al.[19] pointed out that force signal monitoring can reflect machining condition and predict over-grinding phenomenon, which is effective to monitor average grinding force and acoustic emission signal. Feng[20] experimentally verified the effects of grinding speed, feed rate and depth on grinding force and constructed a theoretical model of grinding force that matched the experimental data. Yan et al.[21] found that force signal changes are closely related to the grinding parameters and significantly reduces grinding force and improves machining smoothness. Cao[22] revealed the law of grinding force variation with parameters and the abnormalities can be detected in time by monitoring the grinding force to ensure a smooth machining process. Chi et al.[23]disclosed that the grinding force was linearly proportional to the amplitude of acoustic emission signal change during the grinding process and found that there was a specific relationship model between the acoustic emission signal and the grinding process parameters. Yin et al.[24] found that the acoustic emission signal intensity is directly related to the grinding force and cutting

volume, the grinding wheel speed affects the signal characteristics, and the spectral amplitude varies with the grinding parameters.

From literature, although many domestics and foreign scholars have focused on measurement and modeling of the grinding force, the relationship between the grinding force and grinding wheel characteristics, and the relationship between grinding force and grinding parameters for conventional grinding wheel machining of titanium alloy[25-27], very few efforts have been noted to investigate the grinding force and performance of the small grinding wheel with micro-array structure (SGW-MAS). Compared with the conventionally small grinding wheel, the grinding contact area of structured grinding tools is small, and the micro-array structures on the surface can contain chips and facilitate coolant to enter the grinding zone, resulting in different grinding forces in the machining process. Therefore, the grinding force model of for titanium alloy TC4 using small grinding wheel with micro-array structure is established and the effects of grinding process parameters and grinding wheel structural parameters have been disclosed. It is of great significance to carry out the research on the theoretical modeling of grinding force and the law of force action of the new grinding wheel for the realization of controllable and predictable grinding of titanium alloy.

2. Establishment of grinding force model for SGW-MAS

Compared with the conventional grinding wheel, the grinding contact area of the new grinding wheel is small and there is a micro-array structure on the surface that accommodates chips and facilitates the entry of coolant into the grinding zone, resulting in a different role of the grinding force in the machining process. Therefore, it is of great significance to carry out the theoretical modeling of the grinding force of the new grinding wheel and

research on the law of the chemothermal coupling action for the realization of the controllable and predictable grinding of titanium alloy TC4.

The morphology model of regular array abrasives is divided into three parts: (I) analysis of the surface structure of regular array abrasives; (II) modeling analysis of abrasive particles; (III) determination of the random distribution position of abrasive particles considering the actual parameters of regular array abrasives. For the modeling of abrasive grain, the curved-top quadrangular pyramid model is selected as shown in Fig.1, combined with the reference[28], the sharpness of abrasive grain can be set to about 0.02 times of the wear particle size d_g. The shape of wear particles established is a curved-top quadrangular pyramid with an angle θ_g of 60 degree and the height of cone body is d_g as shown in Fig.1(b).The chord length of the top part of the curve is $0.02d_g$ and the radius is r (r=$0.01d_g$/cos30°), and d_g can be calculated. In order to obtain the random position of the abrasive grain, according to Fig.1(b), the surface of grinding tool is expanded in three dimensions, and the surface of the grinding tool is dispersed into n_g cubic units with L_{cube} side length. The total area occupied by the abrasive grains should be less than or equal to the surface of the abrasive tool in a regular array structure. The n_g should satisfy the following conditions:

$$\sum_{k=1}^{n_g}\frac{\pi}{3}\left(d_{g,k}\right)^2 \le S_{GT} \;\;\&\;\; \sum_{k=1}^{n_g+1}\frac{\pi}{3}\left(d_{g,k}\right)^2 \ge S_{GT} \quad (n_g = 1,2,3.....) \tag{1}$$

Where the S_{GT} represents surface area of regular array structure abrasives.

The cube unit in the i direction along the grinding tool circumference is denoted as i=1,2,……, N_r, and the cube unit in the j direction along the circumference of the grinding tool is marked as j=1,2,……, N_l.Then, the abrasive

grains on the surface of grinding tool with regular array structure can be expressed as G_{ij}. Since the groove structure corresponds to the smaller central angle θ, it is considered that the corresponding central angle of a single abrasive particle in the groove is equal to the central angle of a single abrasive particle in region without groove $\Delta\alpha$. The random placement of abrasive grains on the surface of a regular array structure can be obtained by the following: In the first step, the abrasive grains are uniformly arranged in the center position of the discrete cube unit (x_g, y_g, z_g); In the second step, considering that the abrasive grains on the surface of the abrasive tool are not uniformly distributed but randomly distributed, as shown in Fig.1(c).

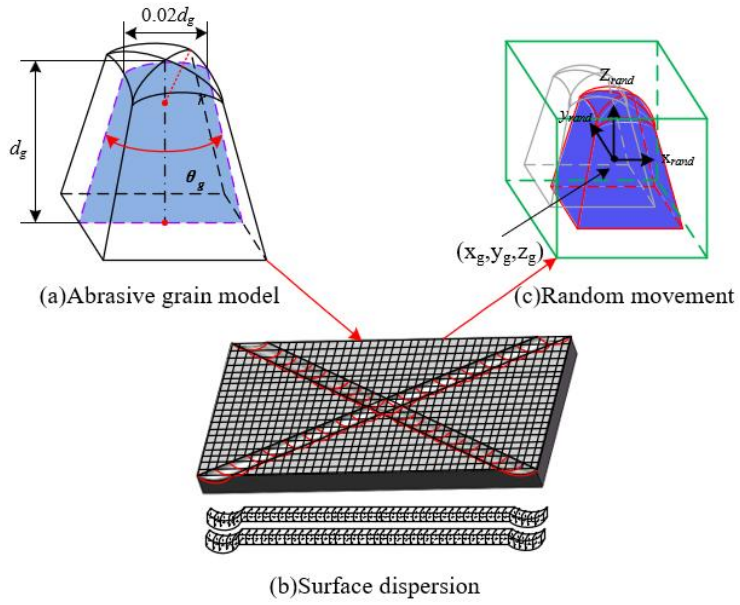


Fig. 1 Modeling process of the random grinding tool with regular array structures topography

Based on the first step, the abrasive grains in the center of the cube unit are randomly moved x_{rand}、y_{rand}、z_{rand} in the *xyz* direction respectively（-0.5L_{cube} ≤x_{rand}、y_{rand}、z_{rand}≤0.5L_{cube}). The third step is to ensure that the abrasive grains do not interfere in the arrangement process. If the interference occurs, the values of x_{rand}、y_{rand} and z_{rand} will be re-assigned .Before analyzing the grinding

force model of a single abrasive grain, it is necessary to analyze the classification of static effective abrasive grains, the dynamic effective abrasive grains, and the contact state between abrasive grains and the workpiece. The grinding force model of one single grain is the basis of the multi-grain grinding force model[29]. In this paper, the grinding force model is established based on the instantaneous contact state between the grain and workpiece and combined with shape of the curved quadrangular cone. The grinding force analysis diagram for the small grinding wheel with micro-array structure is shown in Fig.2. The interference between the abrasive grain and the workpiece in the friction stage occurs at the interface between the abrasive grain and the workpiece surface as displayed in Fig.3. Since the tip of the model is a sphere with radius r, the normal friction in the friction stage can be solved by Hertz contact theory. Based on Herz contact theory[30], the normal friction force $F_{\mathrm{nr},ij}$ and tangential friction force $F_{\mathrm{tr},ij}$ is obtained by Eqs(2) and (3),respectively.

$$F_{\mathrm{nr},ij} = \frac{4}{3} E^{*} \left(\frac{d_{g,ij}}{2} \right)^{2} \left(h_{t,ij} \right)^{3/2} \tag{2}$$

$$F_{\mathrm{tr},ij} = \mu_r F_{\mathrm{nr},ij} \tag{3}$$

Where E^{*} is the modulus of elasticity; μ_r is coefficient of friction and $\mu_r = 0.3$ [31].

As shown in Fig.2(b), considering the shape of the abrasive grain, the cross-sectional area of the abrasive grain G_{ij} in the plowing stage during the material removal process is denoted as S_{ij}, and value of S_{ij} is divided into two cases: (I) critical chip thickness in plowing stage $h_{plowing,ij} \le h_{g,ij} < h_{pcutting,ij}$, if instantaneous thickness of undeformed chips $h_{plowing,ij} \le h_{m,ij} < h_{g,ij}$, the cross-

sectional area is $S_{ij,1}$.

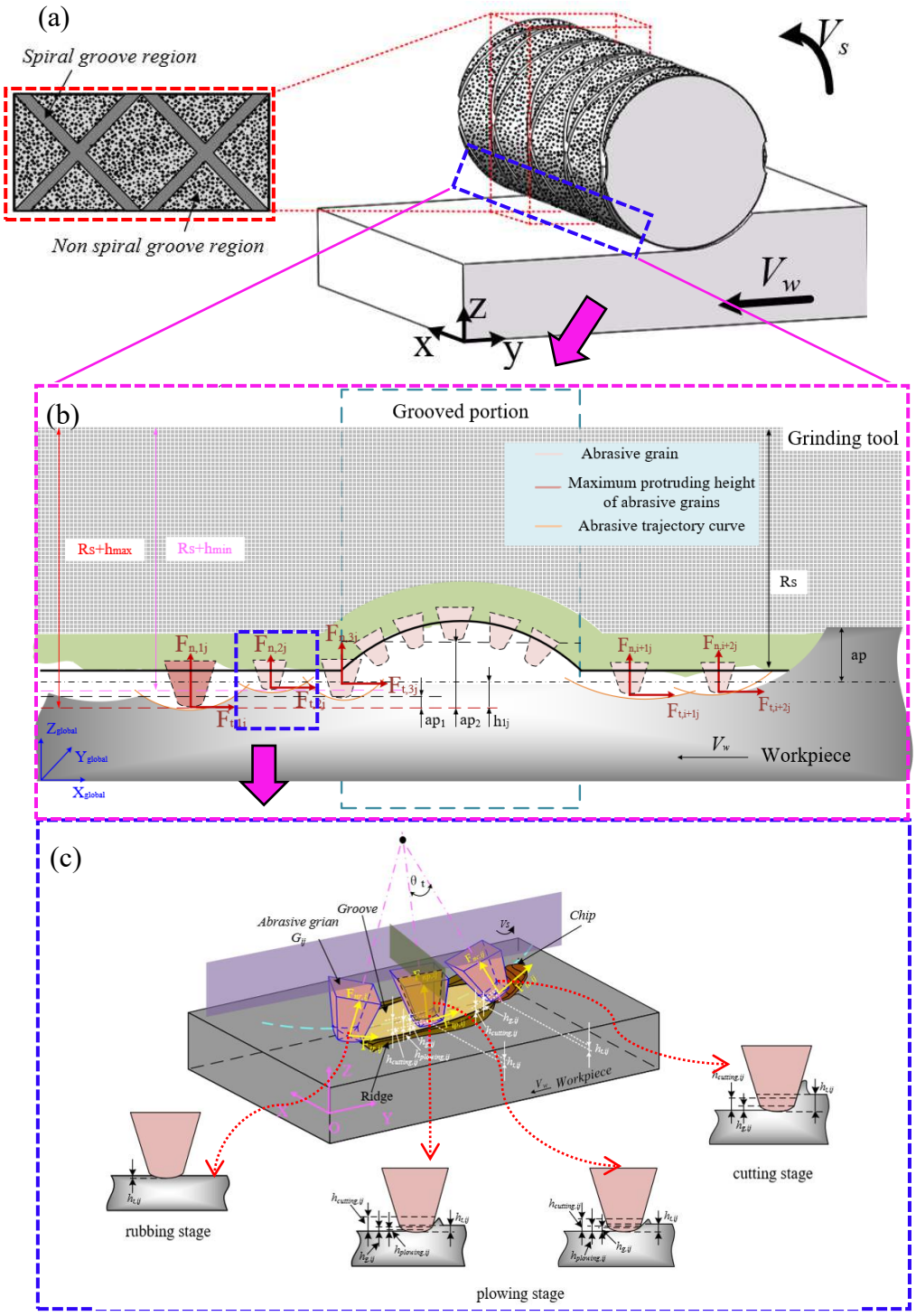


Fig. 2 Schematic diagram of force analysis of multiple grains and force analysis of single grain in three stages

If the instantaneous undeformed chip thickness $h_{g,ij} \le h_{t,ij} < h_{cutting,ij}$,and the

cross-sectional area is $S_{ij,2}$; (II) the critical chip thickness in the plowing $h_{g,ij} \le h_{plowing,ij}$, if instantaneous undeformed chip thickness $h_{plowing,ij} \le h_{t,ij} < h_{cutting,ij}$, the cross-sectional area is $S_{ij,3}$. Therefore, the cross-sectional area of the abrasive G_{ij} in the plowing stage during the material removal process is denoted as S_{ij} and can be expressed as Eq.(4).

$$S_{ij} = \begin{cases} S_{ij,1} = \pi r_{ij}^2 \dfrac{\arcsin(\frac{r_{ij} - h_{t,ij}}{r_{ij}})}{360^\circ} & h_{g,ij} > h_{plowing,ij} \text{ and } h_{t,ij} < h_{g,ij} \\ S_{ij,2} = \dfrac{\pi r_{ij}^2}{3} + \left[r_{ij} \cos\dfrac{\theta_g}{2} + (h_{t,ij} - r_{ij} + r_{ij} \sin\dfrac{\theta_g}{2}) \right] (h_{t,ij} - r_{ij} + r_{ij} \sin\dfrac{\theta_g}{2}) & h_{g,ij} > h_{plowing,ij} \text{ and } h_{t,ij} \ge h_{g,ij} \\ S_{ij,3} = \dfrac{\pi r_{ij}^2}{3} + \left[r_{ij} \cos\dfrac{\theta_g}{2} + (h_{t,ij} - r_{ij} + r_{ij} \sin\dfrac{\theta_g}{2}) \right] (h_{t,ij} - r_{ij} + r_{ij} \sin\dfrac{\theta_g}{2}) & h_{g,ij} \le h_{plowing,ij} \text{ and } h_{plowing,ij} \le h_{m,\theta_{ij}} < h_{cutting,ij} \end{cases} \tag{4}$$

For the plowing force, De Vathaire et al.[32] studied the plowing model, and the normal plowing force equation of a single abrasive grain can be expressed as Eq.(5).

$$F_{\mathrm{tp},ij} = H_s S_{ij} \tag{5}$$

Where H_s is the scratch hardness and H_s=1.08H_v[33]. The indentation shape left by abrasive grain G_{ij} passing through the workpiece can be regarded as the shape of the abrasive grain. In the curved pyramid abrasive grain model established in this paper, the length of the height of the curved top in the direction of the height of the abrasive particle is $h_{g,ij}(h_{g,ij} = r_{ij} - r_{ij} \sin 0.5^* \theta_g)$. Similarly, the indentation width on the workpiece is also divided into two cases: (I)The critical chip thickness in plowing stage $h_{plowing,ij} \le h_{g,ij} < h_{pcutting,ij}$, if the instantaneous thickness of undeformed chips $h_{plowing,ij} \le h_{m,ij} < h_{g,ij}$, the indentation width is $L_{ij,1}$, and if the instantaneous undeformed chip thickness

$h_{g,ij} \le h_{t,ij} < h_{cutting,ij}$, the indentation width is $L_{ij,2}$; (II) the critical chip thickness in the plowing stage $h_{g,ij} \le h_{plowing,ij}$, if the instantaneous undeformed chip thickness $h_{plowing,ij} \le h_{t,ij} < h_{cutting,ij}$, indentation width is $L_{ij,3}$. Therefore, the indentation width of the abrasive G_{ij} in the plowing stage during the material removal process is denoted as L_{ij} and can be expressed as Eq.(6).

$$L_{ij} = \begin{cases} L_{ij,1} = 2\sqrt{r_{ij}^2 - (r_{ij} - h_{t,ij})^2} & h_{g,ij} > h_{plowing,ij} \text{ and } h_{t,ij} < h_{g,ij} \\ L_{ij,2} = 2r_{ij}\cos\dfrac{\theta_g}{2} + 2\left[h_{t,ij} - r_{ij}(1-\sin\dfrac{\theta_g}{2})\right]\tan\dfrac{\theta_g}{2} & h_{g,ij} > h_{plowing,ij} \text{ and } h_{t,ij} \ge h_{g,ij} \\ L_{ij,3} = 2r_{ij}\cos\dfrac{\theta_g}{2} + 2\left[h_{t,ij} - r_{ij}(1-\sin\dfrac{\theta_g}{2})\right]\tan\dfrac{\theta_g}{2} & h_{g,ij} \le h_{plowing,ij} \text{ and } h_{plowing,ij} \le h_{m,\theta_{ij}} < h_{cutting,ij} \end{cases} \quad (6)$$

The expressions of plowing friction coefficient $\mu_{p,ij}$ can be estimated from references[34] as presented in Eq.(7). Therefore, the normal plowing force for the grain G_{ij} at the plowing stage can be expressed as Eq.(8).

$$\mu_{p,ij} = \frac{2}{\pi}\left\{\left(\frac{L_{ij}}{d_{g,ij}}\right)^{-2}\sin^{-1}\left(\frac{L_{ij}}{d_{g,ij}}\right) - \left[\left(\frac{L_{ij}}{d_{g,ij}}\right)^{-2} - 1\right]\right\} \quad (7)$$

$$F_{np,ij} = \frac{F_{tp,ij}}{\mu_{p,ij}} \quad (8)$$

As mentioned above, the critical chip thickness when abrasive grain G_{ij} is $h_{cutting,ij}(h_{cutting,ij} = 0.025d_{g,ij})$, while the length of curved height of grain G_{ij} in direction of abrasive particle height is $h_{g,ij}(h_{g,ij} = r_{ij} - r_{ij}\sin 30^\circ)$. As can be seen $h_{g,ij} < h_{cutting,ij}$, the force analysis of a single abrasive grain G_{ij} in the cutting stage is shown in Fig.2(c). The cutting stage is considered to be related to the formation of chips and the removal of workpiece materials.The normal force and tangential force generated by the G_{ij} movement of abrasive grains in the

cutting stage can be expressed as Eqs.(9) and (10)[35].

$$F_{nc,ij} = \frac{\sqrt{28}}{3}(h_{t,ij})^2 HB \tag{9}$$

$$F_{tc,ij} = F_{nc,ij}\mu_{c,ij} \tag{10}$$

Where $\mu_{c,ij}$ is friction coefficient of cutting stage, $\mu_{c,ij} = \pi/4\tan(\theta_g/2)$[36].

As mentioned above, the grinding force model of a single abrasive grain is established based on the instantaneous contact state between the abrasive grain and the workpiece and combined with the shape of the curved pyramid abrasive grain. In order to obtain the multi-grit grinding force model of the regular array structural abrasive tool, the abrasive vertex with the maximum protruding height is taken as the basis. The rules of array structure of abrasive $O_{global}X_{global}Y_{global}Z_{global}$ three-dimensional expansion plan to build the global coordinate system, based on this, single diamond grits instantaneous grinding force can be deduced. Then the grinding force of a single abrasive grain is synthesized by coordinate transformation, and composite grinding force of regular array structure abrasive particle is derived as Eq.(11).

$$\begin{cases} F_n = \sum_{j=1}^{Nl}\sum_{i=1}^{Nr}\left\{\left[F_{(nr,np,nc),ij}\cos\left(\arctan\frac{Z_{t,ij}-Z_{global,ij}}{X_{t,ij}-X_{global,ij}}\right)\right]+\left[F_{(nr,np,nc),ij}\sin\left(\arctan\frac{Z_{t,ij}-Z_{global,ij}}{X_{t,ij}-X_{global,ij}}\right)\right]\right\} \\ F_t = \sum_{j=1}^{Nl}\sum_{i=1}^{Nr}\left\{\left[F_{(tr,tp,tc),ij}\sin\left(\arctan\frac{Z_{t,ij}-Z_{global,ij}}{X_{t,ij}-X_{global,ij}}\right)\right]-\left[F_{(tr,tp,tc),ij}\cos\left(\arctan\frac{Z_{t,ij}-Z_{global,ij}}{X_{t,ij}-X_{global,ij}}\right)\right]\right\} \end{cases} \tag{11}$$

The grinding force simulation process is displayed in Fig.3, which mainly includes the following four steps: firstly, the grinding tool surface topography modeling considering the truncated hexahedral abrasive grain model and the structural characteristics of the new grinding tool with regular array structure; Then, calculating motion trajectory of abrasive particle and distinguishing dynamic effective abrasive particle; Thirdly, distinguishing the

instantaneous state of abrasive grain; Finally, solving the instantaneous grinding force according to the instantaneous state of the abrasive grains.

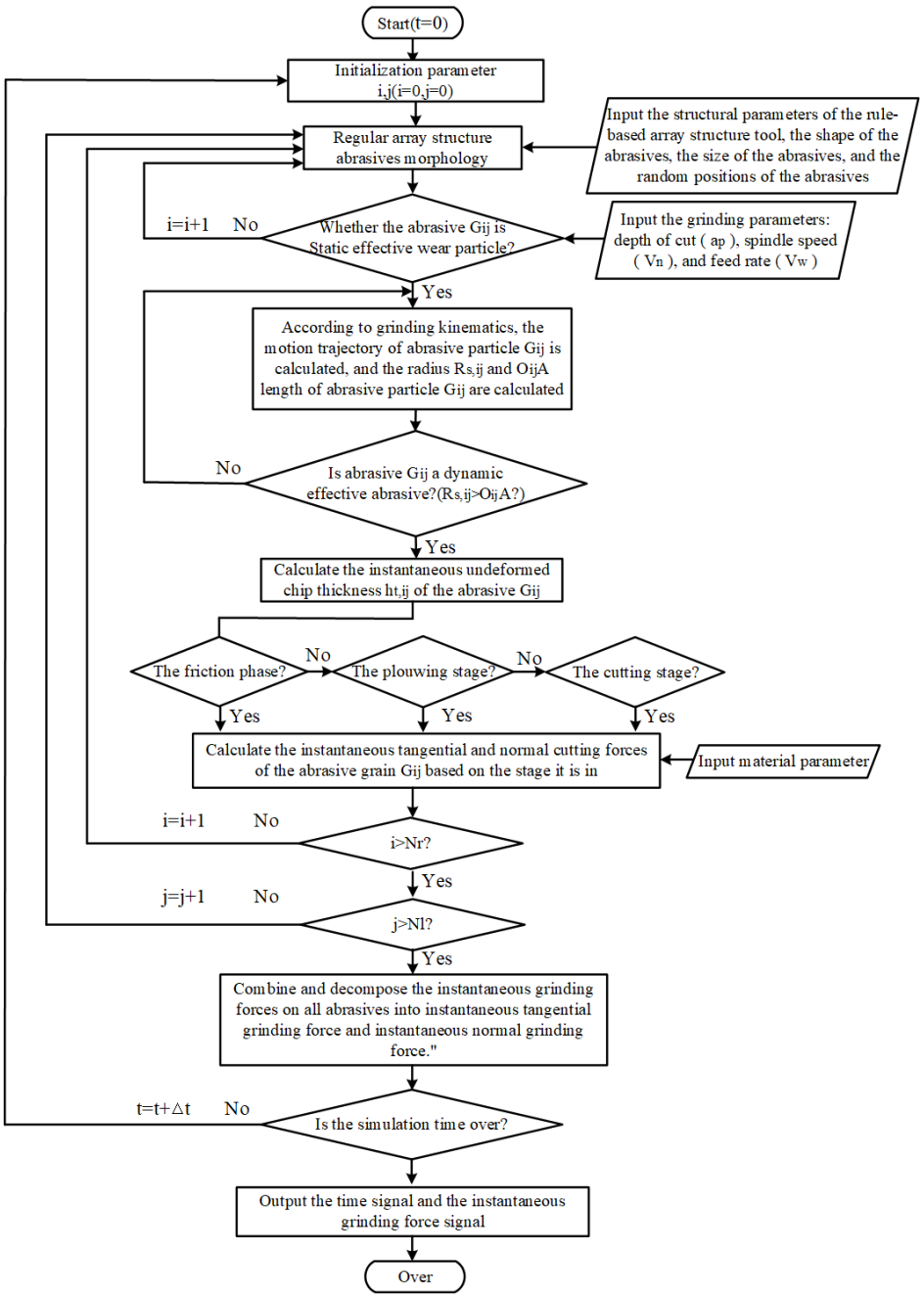


Fig.3. Flow chart of grinding force simulation for SGW-MAS

3. Experimental details

The grinding experiment of titanium alloy TC4 is carried on the JX-1A

precision machine tool manufactured by Shenzhen Juxie precision machinery company as presented in Fig.4, and this machine tool equipped with table workbench size of 560×500mm, spindle speed of 3000~60000rpm, feed speed of 0~1200μm/s, position accuracy of 0.006mm, tool alignment precision of 0.02mm. The workpiece material is titanium alloy (Ti-6Al-4V) and is prepared with the size of 100mm×10mm×10mm. The processing parameters includes rotation speed of 10000~40000rpm, feed velocity of 3~36mm/min, radial depth of 10~40μm, axial grinding depth of 2mm and grinding length of 3mm. Small grinding wheels with micro-array structure made of various abrasive grain size of 300# and 500# and spiral groove depth of 100μm and 200μm are used, respectively. Besides, dry grinding without fluid is adopted to achieve the green machining.

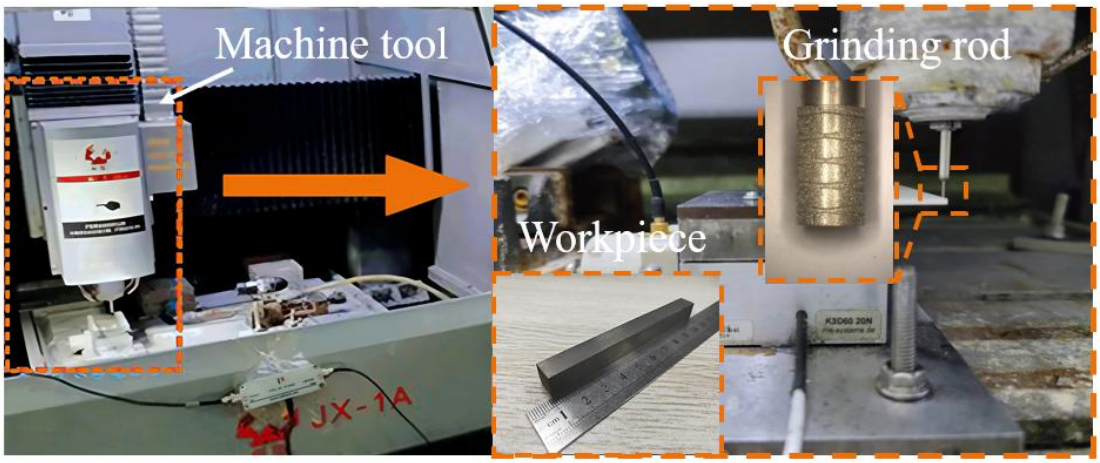


Fig.4. The JX-1A grinding machine tool

Additionally, the grinding force signals are collected by German three-axis dynamometer MEK3D60.This strain-gauge type force instrument has an output signal of 1mV/V, a full-scale interference accuracy of 0.5%, and a range of ±20N in all three directions. It is employed to measure the forces in the *x* and *y* directions during the side grinding process of titanium alloy, and the feed direction is along the *y* axis. The output signals from the force

measuring instrument is conditioned by a strain conditioner and input into the DH5920 dynamic signal testing and analysis system. Then, the eigenvalues of the mean value, standard deviation, peak value and root mean square of titanium alloy grinding force signal are extracted. The surface quality and surface topography of titanium alloy are observed and measured by laser confocal microscope LEXT OLS4100, where the surface roughness parameter values are measured three times and the average value is obtained.

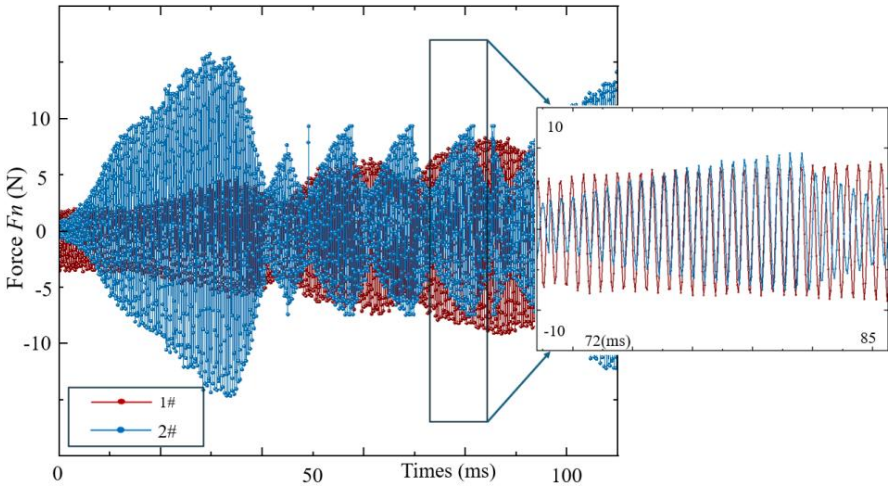
4. Results and discussion

4.1 Influence of geometric structure of small grinding wheel s on grinding force

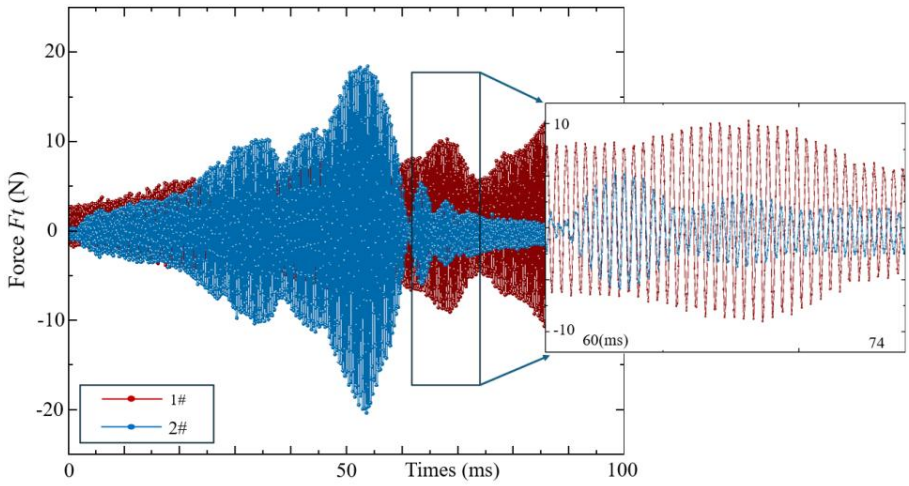
The geometric structure of grinding tools directly affects the grinding force and stability during the grinding process, by optimizing the geometric shape of the grinding wheel's surface, it is possible to reduce the grinding force, improve the stability of the grinding process, and enhance the quality of machining[38-42].Compared to conventional grinding tools, the structured micro-array grinding wheel differs in abrasive particle distribution, grinding contact area, and chip accommodation space, resulting in variations in grinding forces during the process. It is necessary to study the impact of different abrasive grains and surface structural parameters on grinding forces. Therefore, in order to investigate the influences of abrasive grain size and micro groove structure on grinding force are revealed, wherein the groove depth for small grinding wheels 1# and 2# with abrasive grain size of 300 meshes are 100μm and 200μm, respectively; The groove depth of 5# and 6# with abrasive grain size of 500 meshes are 100μm and 200μm, respectively.

The effects of groove depth for SGW-MAS on normal and tangential force signals are investigated as Fig.5, the normal and tangential grinding force of 2# grinding tool

with groove depth of 0.2mm is greater than that of 1# grinding wheel with groove depth of 0.1mm under the same feed speed. This is because the grinding force is the result of the interaction between the grinding wheel and the workpiece, and the increase in the amount of material removed will inevitably lead to the enhancement of this interaction, thus increasing the grinding force; when the groove depth increases, the thickness of the chips generated during the grinding process will also increase, and the increase in chip thickness will require a greater grinding force to overcome the material shear stress and friction resistance. As the groove depth increases, the contact area between the grinding wheel and the workpiece increases accordingly. This means that under the same grinding conditions, more abrasive grains will be involved in the grinding process at the same time. These abrasive grains will work together to exert a grinding force on the workpiece during the grinding process, resulting in an increase in the total grinding force.



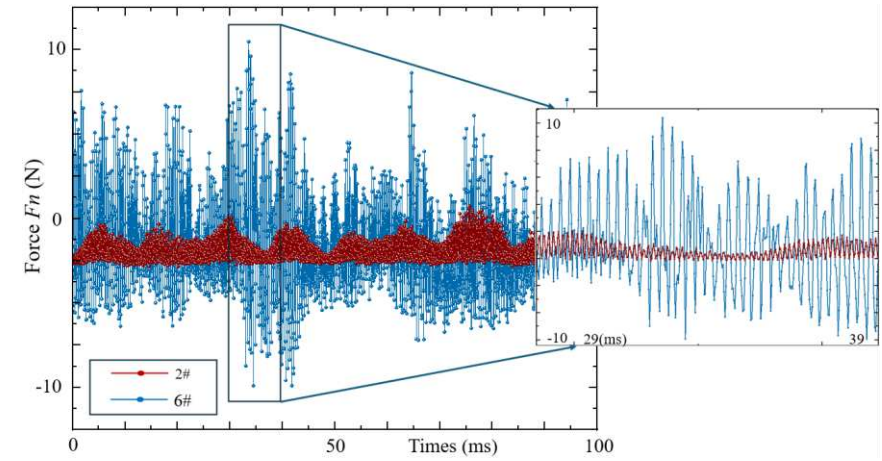
(a) Normal grinding force



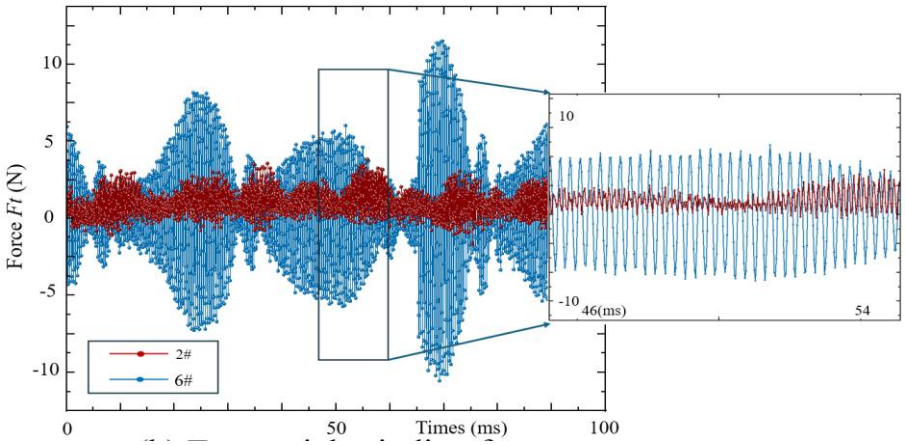
(b) Tangential grinding force

Fig.5. Comparison of grinding force of 1# and 2# SGW-MAS with various groove depth

Effects of abrasive grain size of SGW-MAS on grinding force are analyzed as presented in Fig.8, which indicates that the normal and tangential forces of the 5# and 6# SGW-MAS with abrasive grain size of 500 mesh are less than those of the 1# and 2# SGW-MAS with 300 mesh. This is mainly due to the larger abrasive grain of 300 mesh arise in the larger surface contact area thereby increasing the frictional force. Besides, in the grinding process, the removal of workpiece material by abrasive grains is achieved through micro-cutting actions. Each abrasive grain can be approximated as a tiny cutting edge, and its cutting process is similar to that of a milling cutter's tooth. When the size of the abrasive grain increases, the cutting thickness of each grain also correspondingly increases, meaning that each grain needs to remove more material and the cutting force acting on abrasive grain will increase. Furthermore, the larger abrasive grains may also cause more intense dislocation formation and higher stress concentration, which further increases the fluctuation range of the grinding force as presented in Figs.6(a) and (b).



(a) Normal grinding force



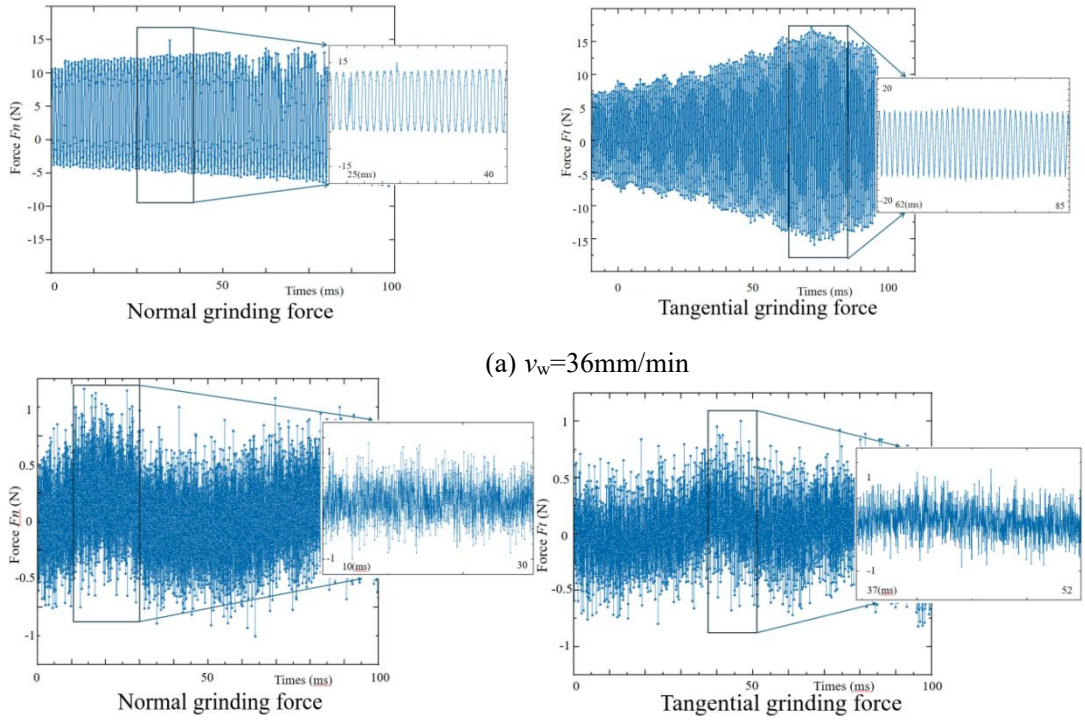
(b) Tangential grinding force

Fig.6. Comparison of grinding force of 2# and 6# SGW-MAS with various abrasive grain size

4.2 Influence of processing parameters of SGW-MAS *on grinding force*

The normal and tangential force signals of TC4 machined by small grinding wheel 1# with various feeding speed are presented in Fig.7, it can be seen that the grinding force for SGW-MAS is increased with the increase of feeding speed, this is mainly due to when feeding speed increases, the relative distance of movement between the grinding tool and the workpiece per unit of time increases, which means that the grinding tool needs to remove more material in the same time. In order to overcome the resistance of this material and remove it from the workpiece, the grinding tool needs to exert a greater force. As the feed rate increases, the speed at which the cutting edge moves across the surface of the workpiece increases. This results in increased friction and compression between the cutting edge and the workpiece, thereby increasing the

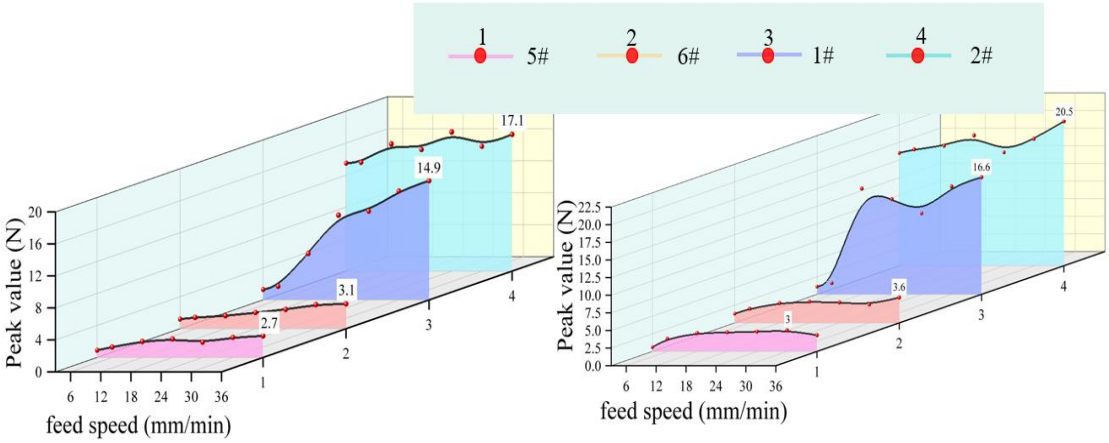
cutting resistance. The increase in cutting resistance is also an important reason for the increase in grinding force.Fig.8 shows the schematic diagram of amplitude variation of normal grinding force and tangential grinding force for 1#, 2#, 5# and 6# at rotating speed n=25000 rpm, cutting depth a_p=12 μm, and feed speed v_w=3mm/min~36 mm/min, respectively. Moreover, as for the 1# and 2# SGW-MAS with 300 abrasive grain size, it can be seen that the normal grinding force of the 1# SGW-MAS reaches the maximum value of 14.9N when the feed rate reaches 36mm/min, the normal grinding force of the 2# SGW-MAS reaches the maximum value of 17.1N when the feed speed reaches 36mm/min. At the same time, the grinding force of 2# SGW-MAS is larger than that of 1#. The tangential grinding force of 1# SGW-MAS reaches a maximum value of 14.6N when the feed speed reaches 36mm/min, and that of 2# SGW-MAS reaches a maximum value of 20.5N when the feed speed reaches 36mm/min. The trend of the tangential force and normal force changes with the feed rate is consistent.



(a) v_w=36mm/min

(b) v_w=6mm/min

Fig.7. The normal and tangential force signal of 1# grinding wheel with various v_w

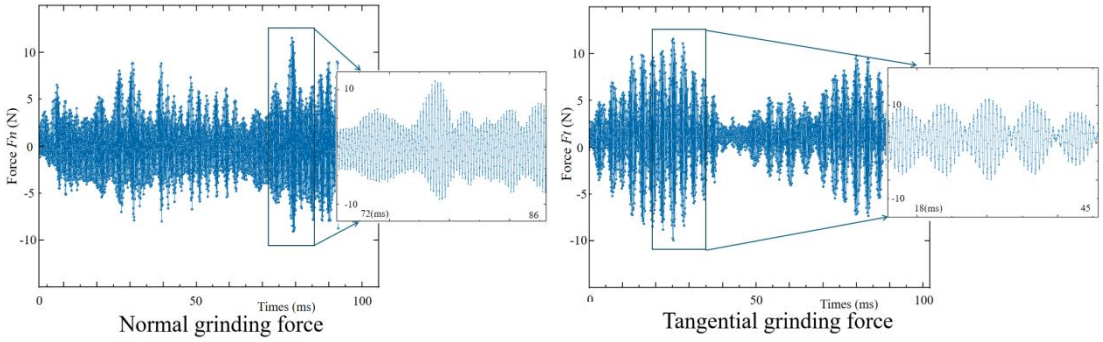


(a)Normal grinding force (b) Tangential grinding force

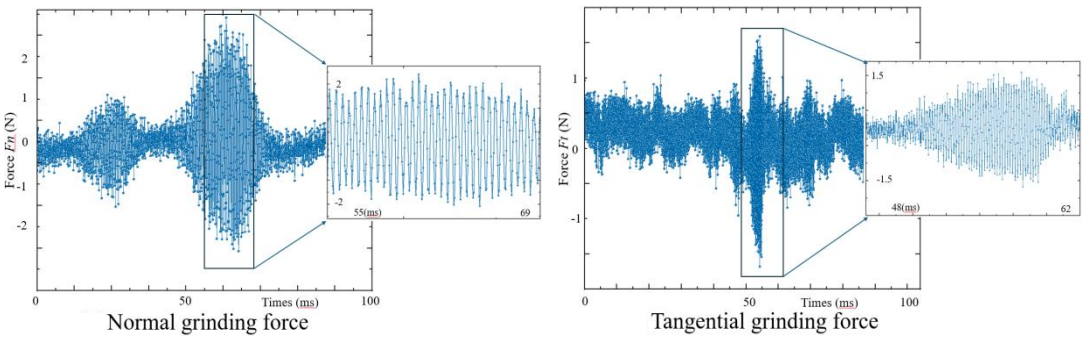
Fig.8. Influence of feed speed on amplitude of grinding force

As shown in Fig.9, the normal and tangential force signal of 1# SGW-MAS with various grinding depth indicated that the grinding force for SGW-MAS obtained with a_p=35μm is obviously larger than that of a_p=10μm.Fig.10 shows the schematic diagram of amplitude variation of normal and tangential grinding force for 1#, 2#, 5# and 6# at rotating speed n=25000 rpm, v_w=12 mm/min and depth a_p=10μm~40μm, respectively. It can be seen that the normal grinding force of the 1# SGW-MAS reaches a maximum value of 10.6N when the grinding depth reaches 35μm, the normal grinding force of the 2# SGW-MAS reaches a maximum value of 10.4N when the grinding depth reaches 35μm. At the same time, grinding force of the 1# SGW-MAS is overall larger than that of the 2# SGW-MAS. The tangential grinding force of 1# SGW-MAS reaches the maximum value of 10.8N when the grinding depth reaches 35μm, the normal grinding force of 2# SGW-MAS reaches the maximum of 9.2N when grinding depth reaches 40μm. The normal and tangential grinding force for titanium alloy TC4 machined by SGW-MAS is increased with the increase of grinding depth. This is mainly due to the increase of the cutting depth directly leads to an increase in the contact area between the grinding wheel and the workpiece during the grinding process. At the same feed speed and wheel speed, a larger contact area means that more material needs to be removed, so the grinding force will increase accordingly; with the increase of the cutting depth,

the depth of the tool in the workpiece is also increases, which leads to an increase in resistance during the cutting process, cutting resistance mainly comes from the shear strength and hardness of the workpiece material, as well as friction between the grinding wheel and the workpiece. The greater the depth of cut results in larger resistance and grinding force. Based on the analysis above, it can be concluded that when the abrasive grains are larger, the average tangential and normal forces for deeper grooved SGW-MAS respectively are 10.64N and 9.47N, which are higher than those of shallower grooved SGW-MAS with tangential and normal grinding forces of 9.14N and 8.28N. As for smaller abrasives, the average tangential and normal forces for deeper grooved SGW-MAS (2.31N and 1.72N) are smaller than than of shallower grooved SGW-MAS (2.38N and 2.01N).

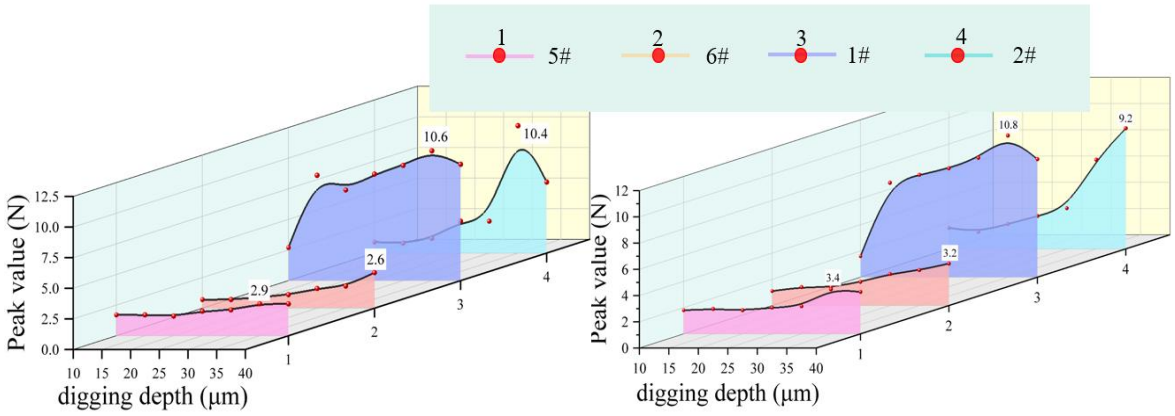


(a) a_p=35μm



(b) a_p=10μm

Fig.9. The normal and tangential force signal of 1# grinding wheel with various a_p



(a)Normal grinding force (b) Tangential grinding force

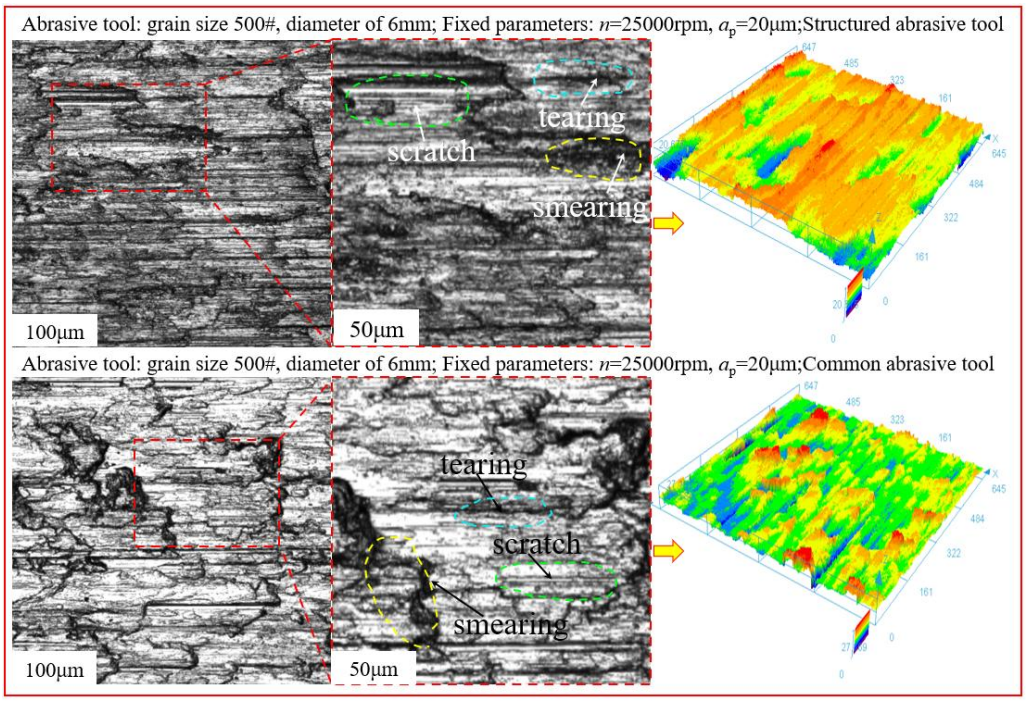
Fig.10. Influence of depth on amplitude of grinding force

4.3 Surface topography for TC4 machined by SGW-MAS

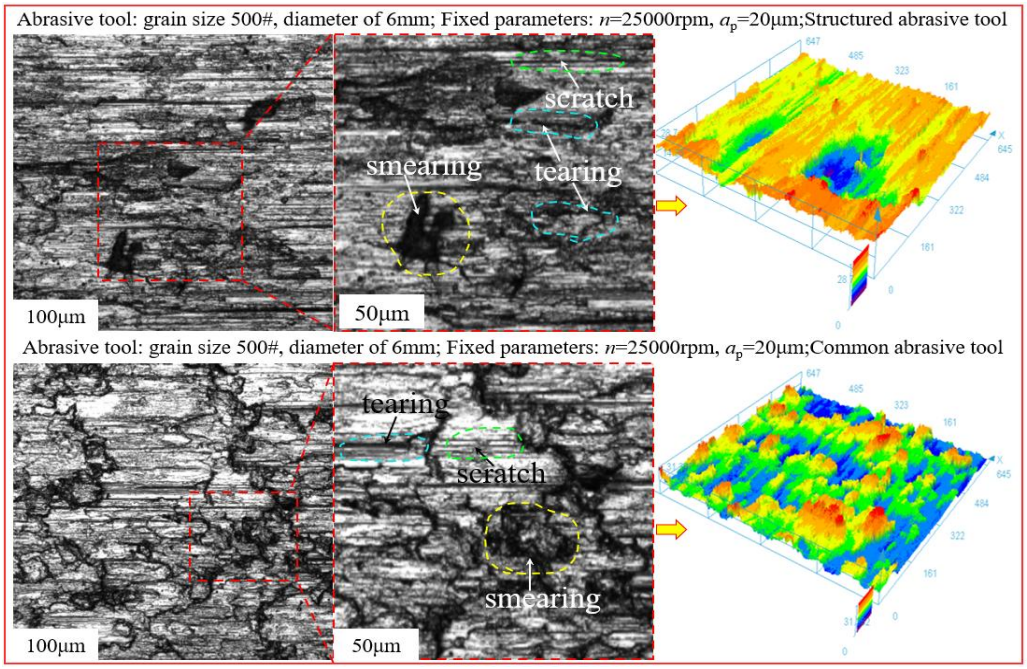
4.3.1 The comparison of surface topography machined by SGW-MAS and ordinary grinding tool

The surface topography after machining has a significant impact on usability performance of parts and components directly affecting the friction coefficient, wear resistance, fatigue life and fracture resistance[43-46].In order to explore the surface characteristics of titanium alloy TC4 workpiece machined by SGW-MAS, the structured grinding tool with the abrasive grain size of 500 mesh and the ordinary grinding tool with the abrasive grain size of 500 mesh are adopted. The comparison of the surface characteristics of the titanium alloy TC4 workpiece machined with various feeding speeds is analyzed as displayed in Fig.11, it can be seen that at the feed speed v_w=6mm/min, both the surfaces of titanium alloy TC4 workpiece machined by SGW-MAS and ordinary grinding tool have appeared scratches, tears, adhesion accumulation and coating phenomenon. But the coating phenomenon of titanium alloy TC4 workpiece machined by SGW-MAS is smaller than that of ordinary grinding tool. Compared with ordinary grinding tool, when feed speed v_w is increased to 36mm/min,

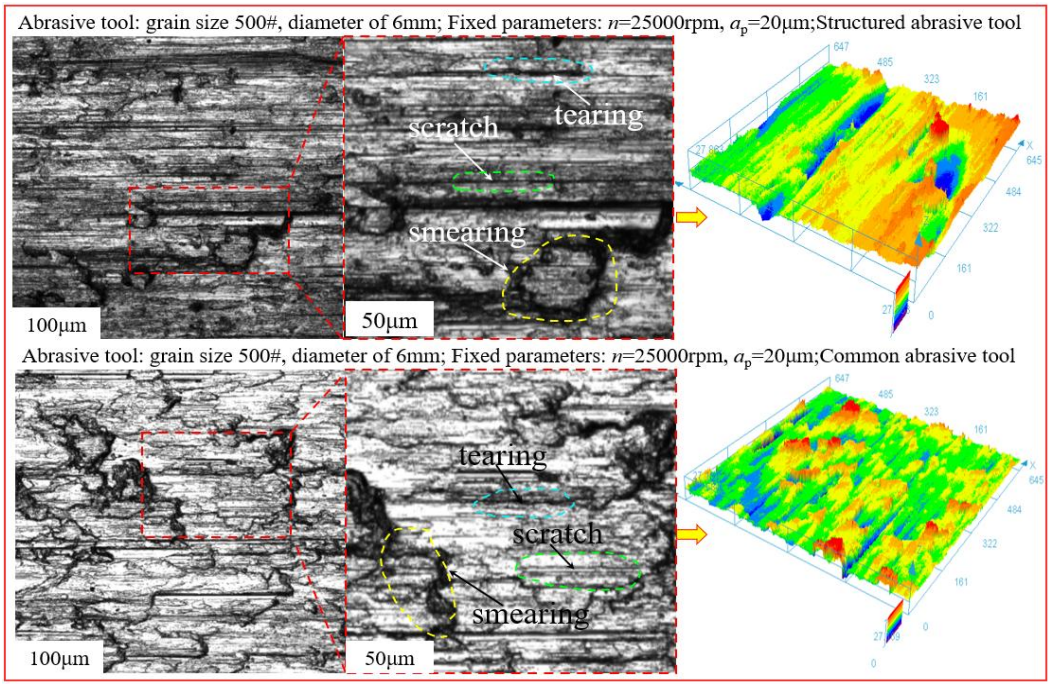
the severity of coating phenomenon of titanium alloy TC4 workpiece surface obtained by SGW-MAS is increased.The reasons why the surface quality machined by structured grinding tool is better than that of ordinary grinding tool are as follows: ordinary grinding tool is prone to accumulate heat and debris during the grinding process, and as the heat and debris stay inside the abrasives for a long time, they are not easy to be discharged from grinding tool, which increases the chances of thermal deformation of the surface of the workpiece as well as surface coating by chips. The structured grinding tool helps to discharge the heat and chips generated during the grinding process, which reduces the risk of thermal deformation and burns on the surface of the workpiece. At the same time, the spiral grooves on the SGW-MAS can make the abrasive particles more evenly distributed during the grinding process, thus reducing the scratches and coating on the surface of titanium alloy TC4 workpiece .



(a) v_w=6mm/min



(b) v_w=18mm/min



(c) v_w=36mm/min

Fig.11. The comparison of the surface characteristics of the titanium alloy TC4 workpiece machined with structured and ordinary grinding tool

4.3.2 The effects of grinding force on surface topography machined by SGW-MAS

The magnitude of the grinding force directly influences the interaction between the grinding wheel and the workpiece during the grinding process, thereby affecting the

roughness of the machined surface[47-48]. Changes in the grinding force also impact the wear state of the grinding wheel and the distribution of abrasive grains, which indirectly affects the surface roughness. When the grinding force is moderate, the grinding wheel can maintain a stable wear state and a uniform distribution of abrasive grains, which helps to achieve better surface quality. The size and direction of the grinding force determine the primary mechanism of material removal; larger grinding forces are usually accompanied by higher cutting temperatures, which may cause thermal damage to the workpiece surface, such as burning or oxidation, thereby reducing surface integrity.

In order to investigate effects of grinding force on surface microtopography of TC4 workpiece machined by SGW-MAS, the structured grinding tool with large and small grain sizes are adopted, respectively. The comparison of surface topography of TC4 workpiece obtained with various grinding forces are presented in Figs.13 and 14. As shown in Fig.12, it can be seen that the surface topography of TC4 workpiece machined by SGW-MAS with 300 meshes is characterized with scratches, tears and abrasive chip adhesion. As grinding force increases, the scratches, grooves, and fish scale-like coating phenomena on the ground surface intensify. This is because larger grinding forces cause more intense interactions between the abrasive particles on the grinding wheel and workpiece, resulting in more scratches and grooves. Additionally, as the grinding force increases, the heat generated during the grinding process also rises. If this heat cannot be dissipated by the coolant in time, it will lead to fish scale-like coating textures on the surface of the workpiece.

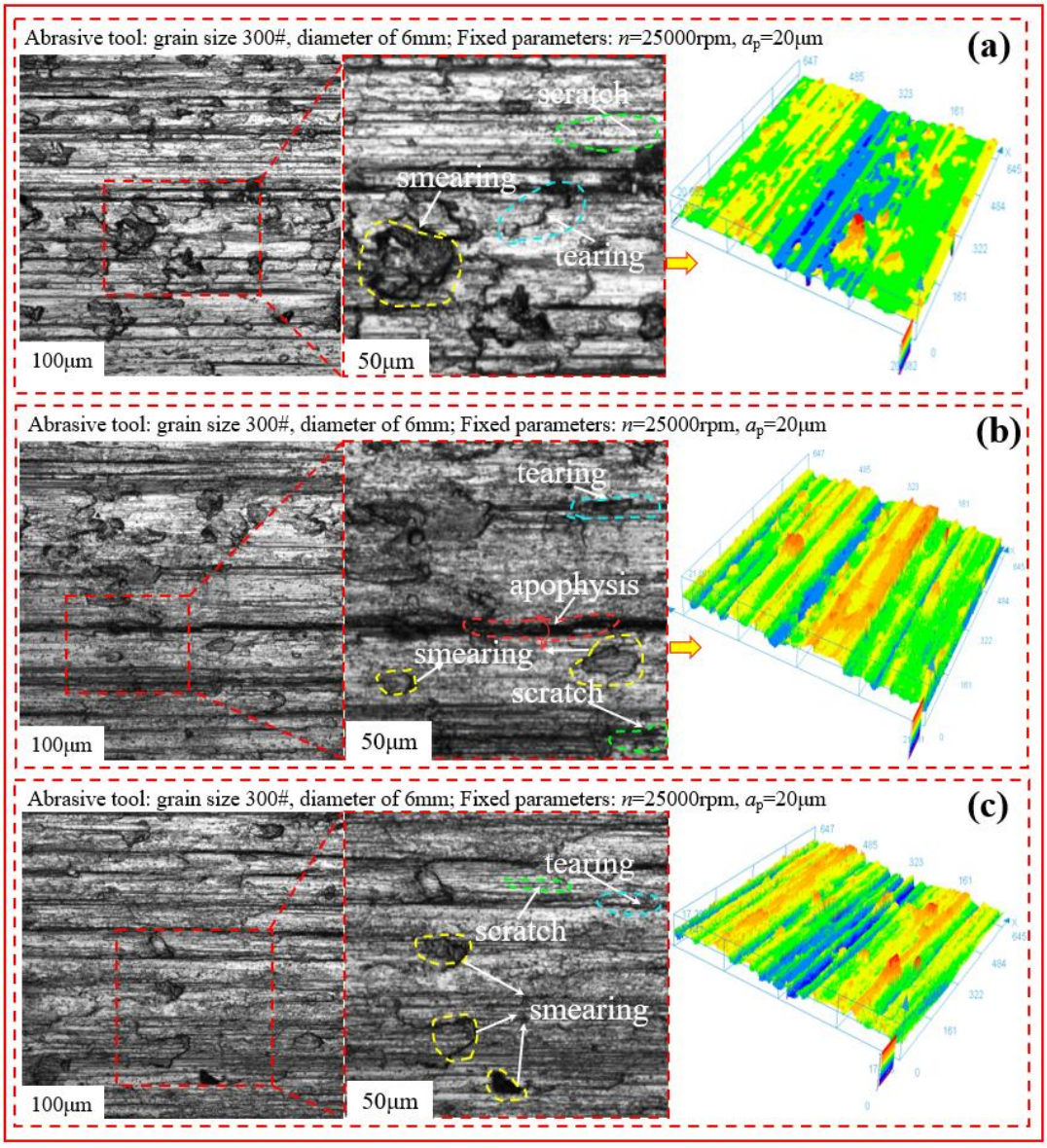


Fig.12. Influence of average grinding force on surface quality machined by SGW-MAS with large grain sizes (a) F=13.6N;(b) F=15.2N;(c) F=17.1N

The surface topography of TC4 workpiece machined by SGW-MAS with 500 meshes is presented in Fig.13, the severity of scratches, tears and coating is decreased compared with surfaces machined by SGW-MAS with 300 meshes.This occurs because of the abrasive grains on the SGW-MAS with 300 meshes is relatively coarse and has strong cutting effect, which easily leads to plastic deformation or micro-cracks on the surface of the workpiece, while the coarse abrasive grains of the crushing speed is fast,

reducing the efficiency of the grinding. In contrast, the cutting effect of the fine abrasive grains of SGW-MAS with 500 meshes is weaker, the surface material of the workpiece is removed more evenly, the generation of plastic deformation and micro-cracks is reduced, the number of repeated processing is reduced, and the processing efficiency is improved.

The surface topography of TC4 workpiece machined by SGW-MAS deteriorates with the increase of the grinding force are as follows: with the increase of the grinding force , the friction and extrusion between the abrasive particles and the workpiece are intensified, resulting in more scratches and plastic deformation on the workpiece surface, which significantly deteriorates the surface quality; The increase in grinding force also leads to an increase in the amount of heat generated during the grinding process, and the grinding temperature increases, and the excessively high grinding temperature will cause the surface of the workpiece to undergo thermal deformation, and even produce burns. With the increase in grinding force , the wear rate of abrasive grains of SGW-MAS will also be accelerated. Worn abrasive grains in the cutting process can not effectively remove material on surface of TC4 workpiece, but will produce more scratches and burrs on the surface of the workpiece, which also reduces the surface topography of grinding.

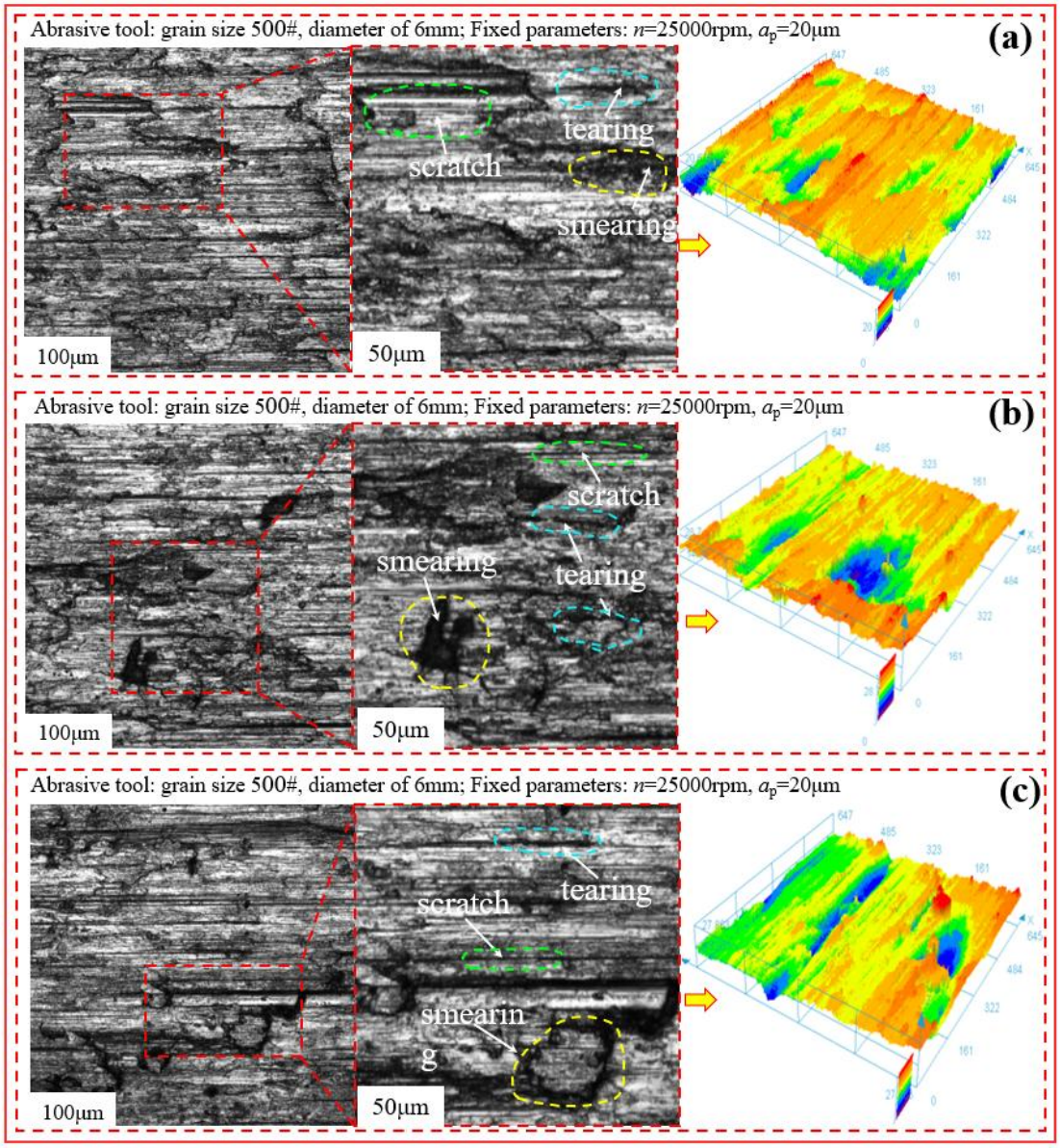
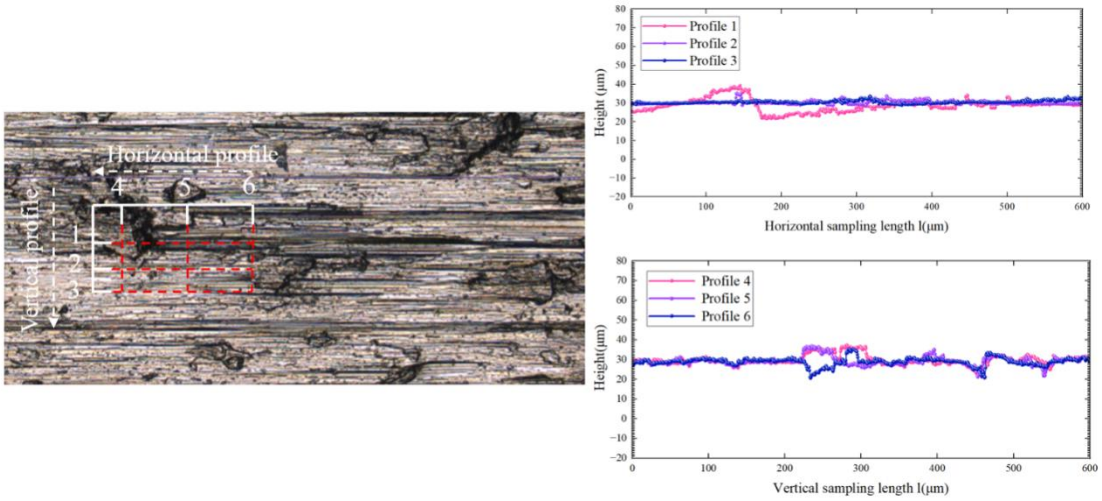


Fig.13.. Influence of average grinding force on surface quality machined by SGW-MAS with small grain sizes (a)F=1.4N;(b) F=2 N;(c) F=3.1N

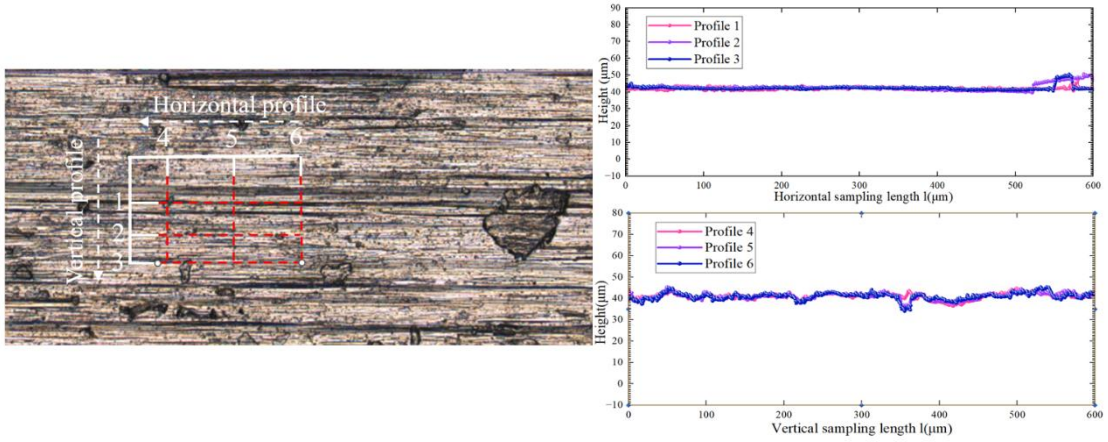
4.4 Relationship of force and surface quality for TC4 machined by SGW-MAS

The surface profile and surface roughness of titanium alloy TC4 obtained by SGW-MAS and ordinary grinding tools with rotating speed n=25000rpm, depth of cut a_p=40μm and feed rate v_w=20mm/min are investigated as shown in Fig.14. For structured grinding wheels, the difference in the cross-sectional profiles of titanium alloy TC4 surfaces parallel and perpendicular to the grinding wheel's feed direction is

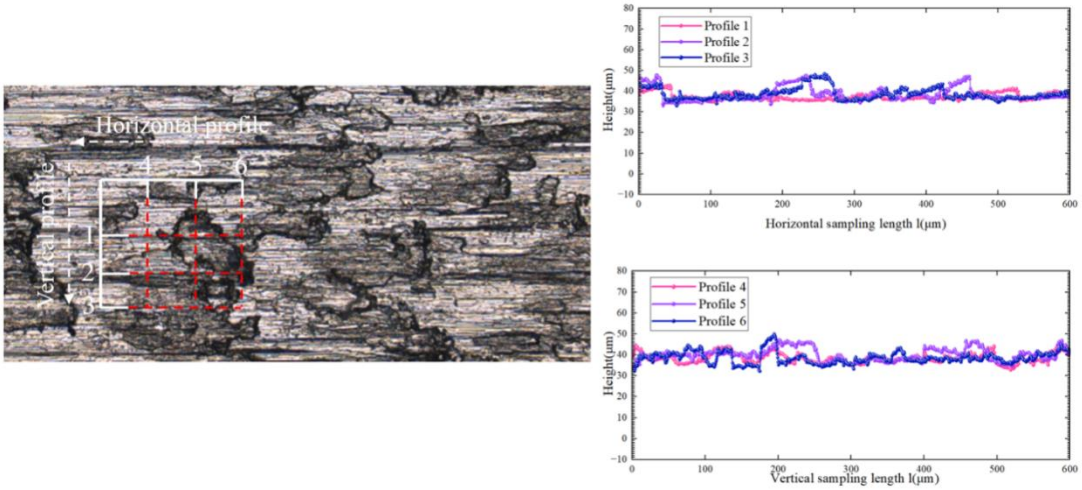
significant, however, for ordinary grinding tools, this attribute is not as pronounced. When parallel to the grinding wheel's feed direction, the grinding marks are shallower and more uniformly distributed, resulting in a relatively lower surface roughness and finer surface texture. This is because the rotation of the grinding wheel aligns with the feed direction, leading to more uniform grinding forces. When perpendicular to the grinding wheel's feed direction, the grinding marks are deeper and less uniformly distributed due to the rotation of the grinding wheel being perpendicular to the feed direction, causing non-uniform grinding forces. As for TC4 workpiece machined by ordinary grinding tools, the surface profiles parallel and perpendicular to the grinding wheel's feed direction both exhibit significant fluctuations, this is due to the difficulty of abrasive debris discharging results in intensified friction and extrusion in the grinding area and appears fish-scale-like coating, so the surface profiles pronounced contour undulations. Moreover, the average surface roughness Ra of TC4 workpiece machined by 5# SGW-MAS, 6# SGW-MAS and ordinary grinding tool respectively are 1.85μm, 1.42μm and 2.36μm. Since the groove depth of 6# SGW-MAS is greater than that of 5# SGW-MAS, which makes it more helpful to discharge the heat and debris generated during the grinding process, so the occurrences of grinding debris cold welding and coating have been successfully mitigated, and the lower the surface roughness of TC4 workpiece can be obtained. The relationship of surface roughness parameters and grinding force machined by SGW-MAS are shown in Fig.15, which indicates that the grinding force and surface roughness are positively correlated.



(a) Surface profile of workpiece ground by 5# SGW-MAS

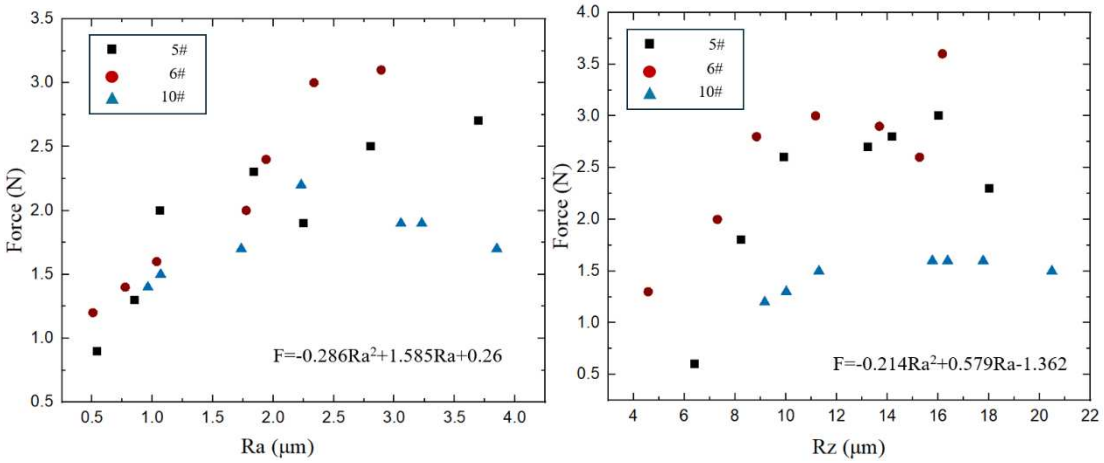


(b) Surface profile of workpiece ground by 6# SGW-MAS



(c) Surface profile of workpiece ground by ordinary grinding tool

Fig.14.. The workpiece surface profile when grinding with different grinding tools



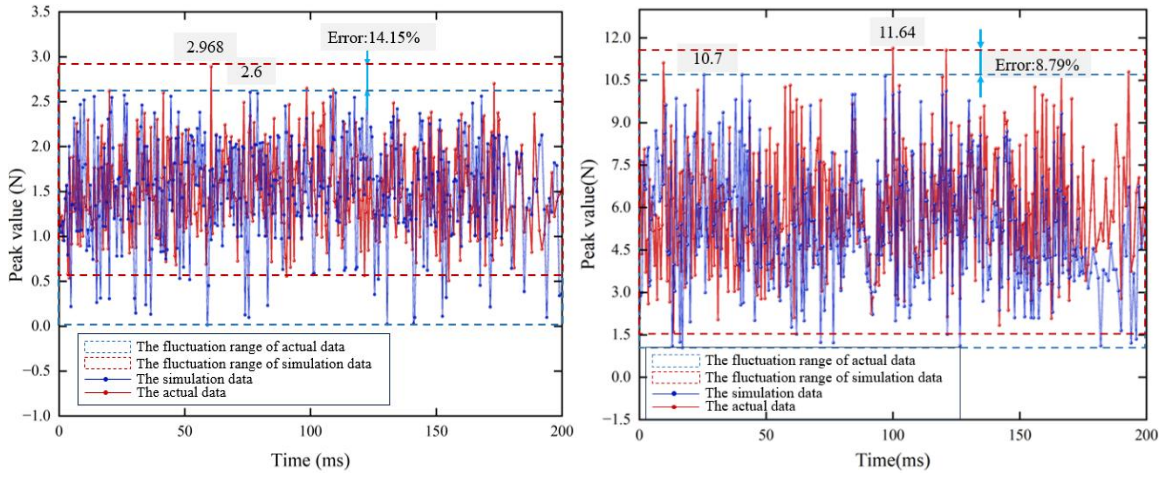
(a) *R*a (b) *R*z

Fig.15. The relationship of surface roughness parameters and average grinding force of TC4 workpiece machined by SGW-MAS

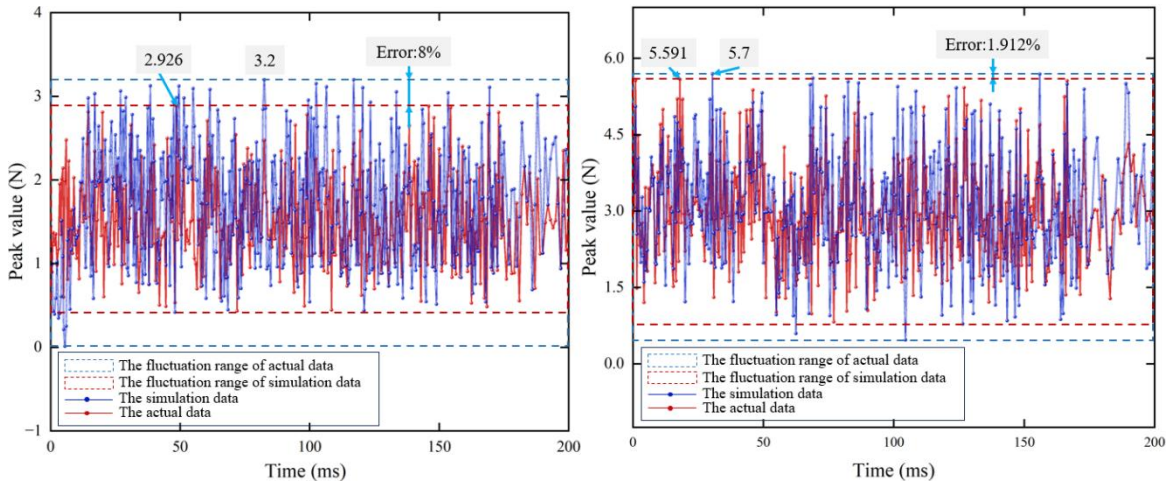
4.5 Comparison of experimental and predicted grinding forces for TC4 machined by SGW-MAS

The comparison of simulation and experiment grinding forces of TC4 machined by SGW-MAS and ordinary grinding tool is displayed in Fig.16, where experimental conditions are the rotational speed of n=25000 rpm, feed speed of v_w= 40 mm/min, and the cutting depth of a_p=20 μm.From the comparative analysis, it can be seen that actual data obtained from the experiment and the simulation results are consistent with the trend of change. 6# grinding tool due to the existence of a regular array structure of grinding force signal change floating compared to the larger, showing a periodic fluctuation. For 6# structured grinding tool, the amplitude of normal grinding force obtained from the experiment is 2.6N, and the amplitude of normal grinding force obtained from the simulation result is 2.968N, with an error of 14.15%; the amplitude of tangential grinding force obtained from the experiment is 3.2N, and the amplitude of tangential grinding force obtained from the simulation result is 2.926N, with an error of 8%. For ordinary grinding tools, under this condition, the amplitude of normal grinding force obtained from the experiment is 10.7N, and the amplitude of normal

grinding force obtained from the simulation result is 11.64N, with an error of 8.79%; the amplitude of tangential grinding force obtained from the experiment is 5.7N, and the amplitude of tangential grinding force obtained from the simulation result is 5.591N, with an error of 1.912%. The error between the actual results and the simulation results is within 20%, which can better respond to the validity of the experimental results. Additionally, Fig.17 shows statistical results of the change of the simulation data and experimental data with the depth for the normal force grinding amplitude and tangential force grinding amplitude of structured grinding tool, and the comparison of simulated and experimental results show that the maximum error in the amplitude of the tangential grinding force is 18.14%, and the maximum error in the amplitude of the normal grinding force is 18.0%. The mean error value of the tangential grinding force is 11.68%, and the mean error value of the normal grinding force is 8.5%. The grinding force model can relatively accurately reflect the actual changes.

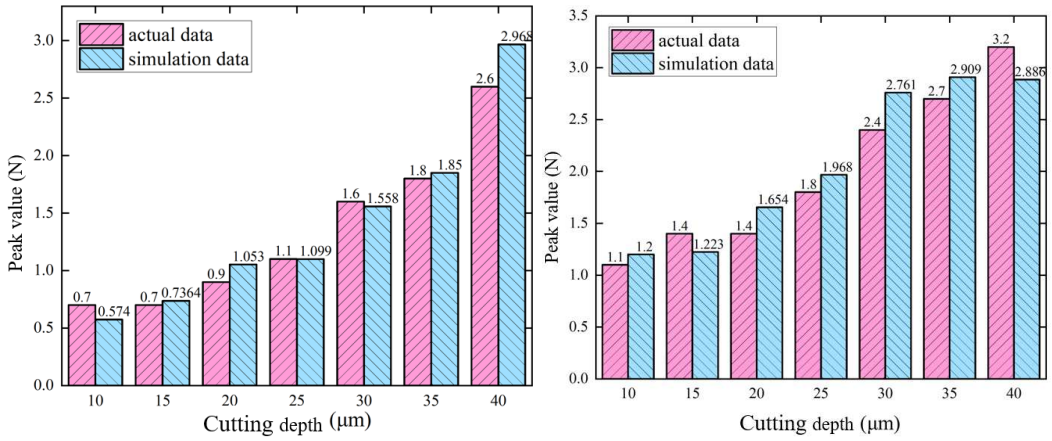


(a) (b)



(c) (d)

Fig.16.. Comparison of grinding forces between simulation and experiment (a) normal force comparison of 6# SGW-MAS; (b) normal force comparison of ordinary grinding tool; (c) tangential force of comparison 6# SGW-MAS; (d) tangential force comparison of ordinary grinding tool



(a) (b)

Fig.17. Statistical comparison between simulation data and experimental data of structured grinding tool (a) the comparison of normal force data; (b) the comparison of tangential force data

Conclusion

The present study attempted to investigate the grinding force model of titanium alloy Ti-6Al-4V machined by structured grinding tools, and the mapping relationship of structured parameters of grinding tool, processing parameters, surface morphology, surface roughness and grinding force in dry grinding process are disclosed . The following conclusions could be drawn from the study:

(1) The grinding force model considering the instantaneous state of abrasive grains, critical chip thickness, and structured tool parameters involved in grinding titanium alloys has been established and experimentally validated.The comparison of simulated and experimental results indicated that the mean error value of the tangential grinding force is 11.68%, and the mean error value of the normal grinding force is 8.5%, which can relatively accurately reflect the actual changes in grinding forces.

(2) The comparative analysis of the grinding forces in dry grinding of titanium alloy TC4 using structured grinding tools with different groove depths and abrasive grain sizes versus conventional grinding tools indicates that the depth of helical grooves significantly affects the dry grinding force on titanium alloys for coarse abrasive grains, however, for fine abrasives, the influence of the helical groove depth is minimal. Similarly, the mean values of tangential and normal grinding forces for structured grinding tools with larger abrasive grains are lower than those with smaller grains. Additionally, the mean values of tangential and normal grinding forces for structured grinding tools are lower than those for grinding tools, which demonstrates that structured grinding tools with regular array can effectively reduce the grinding forces compared to conventional grinding tools during the dry grinding of titanium alloy TC4.

(3) The spiral grooves on the surface of structured grinding tool significantly reduces the fish-scale coating phenomenon on the dry grinding surface of titanium alloys compared to conventional grinding tools.

(4) For structured grinding tools, the difference in the cross-sectional profiles of titanium alloy TC4 surfaces parallel and perpendicular to the grinding wheel's feed

direction is significant, however, for ordinary grinding tools, this attribute is not as pronounced.

Declaration of Competing Interest

The authors declare that they have no known competing financial interests or personal relationships that could have appeared to influence the work reported in this paper.

Data availability

The processed data of this work can not be shared as it forms part of an ongoing work.

Funding

This study was funded by the Open Project of State Key Laboratory for High Performance Tools (GXNGJSKL-2024-07), Fundamental Research Funds for the Central Universities (N26GFZ015), the China Postdoctoral Science Foundation (2024MD754246), National Natural Science Foundation joint fund project of China (U23A20633), Natural Science Foundation of Liaoning Province (2024-MSBA-39); the National Natural Science Foundation of China (No. 52275412); the Fundamental Research Funds for the Central Universities (N25GFZ009).

Reference

[1] MT Ali, Z Jebri, J Jumel (2024) Evaluation of the critical SERR in the presence of heterogeneous interfaces in bonded joints: application to parallel defects in DCB titanium alloy laser-treated specimens. J Braz. Soc. Mech. Sci. Eng. 46:188 .

[2] Feng, R., Chen, M., Xie, L (2023) Research on mesoscopic damage evolution models of TC4 titanium alloy under hot deformed process. J Braz Soc Mech Sci Eng 45:486.

[3] Wu C, Chen C, Li C (2024) Analysis of machined surface quality for multi-feature standard parts. J Manuf Process 115:452-465.

[4] Zhou, Y., Tian, C., Li, H (2022) Study on removal mechanism and surface quality of grinding carbon fiber toughened ceramic matrix composite. J Braz Soc Mech Sci Eng 44:476.

[5] Qu SS, Yao P, Gong YD, Yang YY, Chu DK, Zhu QS (2022) Modelling and grinding characteristics of unidirectional C－SiCs, Ceramics International 48：8314-8324.

[6] Yan B, Zhu L, Dun Y (2021) Tool wear monitoring of TC4 titanium alloy milling process based on multi-channel signal and time-dependent properties by using deep learning[J]. J Manuf Syst 61:495-508.

[7] Ma Z, Wang Q, Chen H, Chen L, Qu S, Wang Z (2022) A grinding force predictive model and experimental validation for the laser-assisted grinding (lag) process of zirconia ceramic. J Mater Process Technol 302:117492.

[8] Qin S, Zhu L, Hao Y (2023) Theoretical and experimental investigations of surface generation induced by ultrasonic assisted grinding. Tribology International 179:108120.

[9] Niu B, Sun J, Yang B (2020) Multisensory based tool wear monitoring for practical applications in milling of titanium alloy. Mater. Today: Proc 22:1209-1217.

[10] Jemielniak K, Arrazola P (2008) Application of AE and cutting force signals in tool condition monitoring in micro-milling. CIRP J Manuf Sci Tech 1:97-102.

[11] Nogi Y, Sakaino S (2022) Contact Force Detection of Grinding Process Using Frequency Information and Differential Feature on Force Signal. IEEE Access 10:127140-17148.

[12] Sakaino S, Tsuji T (2022) Force Control of Grinding Process Based on Frequency Analysis. IEEE Rob Autom Lett 7:3250-3256.

[13] Qin X, Shi M, Hou Z (2022) Analysis of 3-DOF cutting stability of titanium alloy helical milling based on PKM and machining quality optimization. Machines 10:404.

[14] Xavier R, Francois C (2017) Burr height monitoring while drilling CFRP/titanium/aluminium stacks. Mechanics and industry 18.

[15] Kwak J, Ha M (2004) Detection of dressing time using the grinding force signal based on the discrete wavelet decomposition. Int J Adv Manuf Tech 23:87-92.

[16] Wang L, Tian X, Liu Q (2017) Experimental study and theoretical analysis of the form grinding of gears using new type micro-crystal corundum grinding wheels.

Int J Adv Manuf Tech 92:1659-1669.

[17] Sutowski P, Swiecik R (2018) The estimation of machining results and efficiency of the abrasive electro-discharge grinding process of Ti-6Al-4V titanium alloy using the high-frequency acoustic emission and force signals. Int J Adv Manuf Tech 94:1263-1282.

[18] Jamshidi M, Rimpault X, Balazinski M (2020) Fractal analysis implementation for tool wear monitoring based on cutting force signals during CFRP/titanium stack machining. Int J Adv Manuf Tech 106:3859-3868.

[19] Tasi H, Hocheng H (2001) Monitoring strategy of thermal-induced convex deformation of workpiece in surface grinding. Int J Adv Manuf Tech 17:710-714.

[20] Feng R (2022) Research on grinding force of titanium alloy with diamond wheel. Diamond and Abrasives Engineering 42:193-200.

[21] Yan YY, Yan HZ, Liu JL (2023) The coupling model and experimental study of longitudinal torsional ultrasonic grinding of TC4 titanium alloy. Chin J Mech Eng-en 34:65-74.

[22] Cao K, Dong ZG, Kang RK (2016) Study on Grinding Force of Titanium Alloy TC17 with Microcrystalline Corundum Wheel. Diamond and Abrasives Engineering 36:1-7.

[23] Chi YL, Li HL, Lin XK (2014) Research on acoustic emission signal of cylindrical plunge grinding based on grinding force model. Precise Manufacturing and Automation 04:52-55.

[24] Yin GQ, Feng YC, Han HC (2023) Grinding surface roughness model based on acoustic emission and experimental verification. Diamond and Abrasives Engineering 43:640-648.

[25] Chen Li, Kechong Wang, Yinchuan Piao, Hailong Cui, Oleg Zakharov, Zhiyu Duan, Feihu Zhang, Yongda Yan, Yanquan Geng (2024) Surface micro-morphology model involved in grinding of GaN crystals driven by strain-rate and abrasive coupling effects. Int J Mach Tools Manuf 201:104197.

[26] Qin S, Zhu L, Hao Y (2023) Theoretical and experimental investigations of surface generation induced by ultrasonic assisted grinding. Tribology International 179: 108120.

[27] Bo Yan, Ning He, Ni Chen, Matthias Weigold, Huiwen Chen, Shuchen Sun, Yang Wu, Shiyang Fu, Liang Li (2025) Achieving precise graphenization of diamond coatings below the interfacial thermal stress threshold. IJEM 7:015106.

[28] Jackson MJ, Hitchiner MP (2012) High performance grinding and advanced cutting tools. USA: Springer Science & Business Media.

[29] Su C , Zhang Y , Hou JM , Wang WS (2008) Numerical simulation and analysis for metal cutting processes based on FEM and SPH. Simultech 8:1325.

[30] Johnson KL, Johnson KL (1987) Contact mechanics. Cambridge University Press.

[31] Kim N, Guo C,Malkon S (1997) Heat flux distribution and energy partition in creep-feed grinding. CIRP Ann Manuf Technol 46: 227–232.

[32] De Vathaire M, Delamare F, Felder E (1981) An upper bound model of ploughing by apyramidal indenter. Wear 66:55–64.

[33] Williams, J. A. (1996) Analytical models of scratch hardness. Tribology International, 29:675–694.

[34] Sin H, Saka N, Suh N (1979) Abrasive wear mechanisms and the grit size effect. Wear 55: 163–190.

[35] J. Goddard, H. Wilman (1965) A theory of friction and wear during the abrasion of metals. Wear 5:114.

[36] Lawn B, Wilshaw R (1975) Indentation fracture: principles and applications. J Mater Sci 10:1049–81.

[37] Li L, Fu J, Peklenik J (1980) A study of grinding force mathematical model. CIRP Ann Manuf Technol 29:245–9.

[38] Sun Y, YR Sun, YM Huang, S Gong, MS Sun, M Liu(2025). Study on developing predicted system model of cutting-edge trajectory for micro-milling process based on tool runout error, chip thickness and force signal. Mechanical Systems and Signal Processing,228,112410.

[39] Zhou H, Xiao B, Zhou LY, Wang S, He X (2024) Development of multilayer brazed diamond grinding wheel for ceramic precision grinding. Diamond & Abrasives Engineering 44:50-56.

[40] Duan DZ, Zhang W, Liu H, Chen SS, Li CS, Li B, Jing WX, Wang CY, Jiang ZD Effect of PMMA pore former on mechanical strength and performance of glass

fibre metal-bonded porous diamond blocks with Cu – Sn – Ti solder alloys. Diamond and Related Materials 144: 111054.

[41] Ma LJ, Sun ZC, Zhang L, Deng H, Tan YQ, Kong Z, Wei ZQ (2020) Study on mechanism and theoretical model of tool wear in fluorophlogopite glass-ceramics. J Mater Process Technol 275:116284.

[42] Zhao B, Wu BF, Yue YS, Ding WF, Xu JH, Guo GQ (2023) Developing a novel radial ultrasonic vibration-assisted grinding device and evaluating its performance in machining PTMCs. Chinese J Aeronaut 36:244-256.

[43] Zhao B, Song J, Xie L (2023) Multiaxial fatigue life prediction method based on the back-propagation neural network. Int J Fatigue 166:107274.

[44] Sun LF, He ZF, Nan J, Guo YX (2024) Local chemical order enables an ultrastrong and ductile high-entropy alloy in a cryogenic environment. Science Advances 10:1-12.

[45] Li ZQ, Sun ZP, Ding YC (2023) Research on design and fabrication of micro ball end milling tool with flat edge and conical flank. Precis Eng 79323-334.

[46] Sun Y, Jin LY, Gong YD, Wen XL, Yin GQ, Wen Q, Tang BJ (2022) Experimental evaluation of surface generation and force time-varying characteristics of curvilinear grooved micro end mills fabricated by EDM, J Manuf Processes 73:799-814.

[47] ChenSS, Yang SM, Chi F, Cheung, Lai TH, Zhang FH (2022) Suppression strategy of micro-waviness error in ultra-precision parallel grinding. Nanomanuf. Metrol5:423-429.

[48] Li C, Hu YX, Wei ZZ, Wu CJ, Peng YF, Zhang FH, Geng YQ (2024) Damage evolution and removal behaviors of GaN crystals involved in double-grits grinding. Int J Extreme Manuf 6:025103.